PNAS

Main Manuscript for

Amazon forest faces severe decline under the dual pressures of anthropogenic climate change and land-use change.

Selma Bultan[1],Yiannis Moustakis[1],Sebastian Bathiany[2],Niklas Boers[2,3,4],Raphael Ganzenmüller[1], Gergana Gyuleva[5],Julia Pongratz[1,6].

1) Department of Geography, Ludwig-Maximilians-Universität, Germany.
2) School of Engineering and Design, Technical University Munich, Germany.
3) Potsdam Institute for Climate Impact Research, Potsdam, Germany.
4) Department of Mathematics and Global Systems Institute, University of Exeter, Exeter, UK.
5) Institute of Atmospheric and Climate Science ETH Zurich, Switzerland.
6) Max Planck Institute for Meteorology, Germany.

*Selma Bultan.

Email: selma.bultan@lmu.de

Author Contributions: S.B. and J.P. designed the study. S.B. developed the attribution approach with input from J.P., Y.M. and S.B. S.B. conducted the data analysis with input from all authors. S.B. drafted the initial version of the manuscript, and all authors provided critical feedback and helped shape the research, analysis and manuscript.

Competing Interest Statement: The authors declare no competing interests.

Classification: Physical Sciences, Environmental Sciences

Keywords: Amazon rainforest, Climate tipping elements, Climate Change, Land-Use Change

This PDF file includes:

Main Text
Figures 1 to 5
Tables 1 to 3

Abstract

The Amazon is a key climate system component, hotspot of biodiversity and many other ecosystem functions. However, progressive rainforest degradation, driven by anthropogenic climate change and land-use change, is increasing the risk of a large-scale critical ecosystem transition. Previous studies highlight forest vulnerability to isolated or combined climate change and land-use pressures, but have not disentangled individual driver contributions. This crucial knowledge gap needs to be addressed for a holistic understanding of the risks that the rainforest is facing. Combining Earth System Model data with a robust detection and attribution framework, we assess forest decline under individual and combined pressures of climate change and land-use change. We assess abrupt shifts and nonlinearities in local and basin-wide forest decline to reveal signs of resilience loss and potentially imminent forest transitions. We identify land-use change as the dominant driver of past degradation, accounting for 80% of the historical (1950-2014) forest decline. Future projections reveal that up to 38% of the mid-20th century forest area could be lost by 2100, with 25% caused by continued deforestation and 13% caused by unmitigated global warming. Importantly, the risk of abrupt rather than gradual forest decline increases as global warming progresses, with a strong nonlinear trend beyond a threshold of 2.3°. These findings highlight a substantial risk of a large-scale transition, with potentially devastating consequences for the global climate system, regional water and carbon cycles, human livelihoods, and biodiversity. Limiting this risk requires rigorous forest protection and climate mitigation in line with the Paris Agreement.

Significance Statement

The Amazon, the world's largest rainforest and a potential tipping element in the Earth System, faces increasing pressures from deforestation and global warming. Understanding the individual and combined impacts of these pressures is critical for anticipating the risk of widespread forest collapse. Our study offers new perspectives on the effects of land-use change and climate change on forest vulnerability. We identify a global warming threshold of 2.3°C beyond which forest decline accelerates nonlinearly. This is accompanied by a growing risk of abrupt forest loss, indicating a decline in ecosystem functions and resilience. Our findings highlight the need for immediate policy action to prevent cascading ecological and climatic impacts that extend far beyond the Amazon itself.

Main Text

Introduction

The Amazon rainforest ecosystem takes up around 0.3 Pg C per year[1], and therefore contributes substantially to regulating the global climate system by attenuating anthropogenic global warming[1,2]. It further offers unique services by providing water supply at continental scales, hosting biodiversity, and supporting livelihoods[1–4]. Intact Amazonian rainforests 'recycle' moisture through repeated cycles of evapotranspiration with subsequent cloud formation and rainfall[5], strongly increasing the overall amount of available moisture. However, the Amazon is facing a widespread conversion of intact rainforest to degraded forest, savanna and managed land[6–9]. The underlying drivers are direct human activities, primarily through deforestation, and anthropogenic climate change, leading to an increasing number and severity of natural disturbances[6–9]. There is growing concern that these combined pressures might push the rainforest closer to a critical threshold of deforestation, global warming and/or moisture supply. Crossing these critical thresholds could trigger a large-scale transition to a savanna-like or degraded forest state (referred to as 'tipping point')[3,10–14].

Recent analyses of observational data reveal a declining resilience of the rainforest over the past decades[6] and a switch from net CO_2 sink to source in the Southeast of the Amazon[7]. These findings provide alarming evidence that the Amazonian ecosystem might be approaching a critical transition, but substantial conceptual (e.g., the general existence of a tipping point, the most likely alternative stable states)[4,12] and quantitative (e.g., the values of the critical threshold(s), the spatial patterns and timing of forest transitions)[4,12,15] uncertainties remain.

Predicting the future state of the Amazon rainforest and the likelihood of abrupt changes (i.e., changes at a rate much faster than the typical rates for the ecosystem) and transitions requires an analysis of the dual, i.e., individual and combined, impacts of land-use change and climate change. Previous studies have identified deforestation (20-50%)[3,16,17] and global warming (2-6°C)[15] threshold ranges beyond which a large-scale transition of the Amazon rainforest could occur. However, some of these studies only consider the isolated impact of climate change[6,18,19] or land-use change[3,16,20] on the forest. Consequently, they neglect interactions between the drivers – e.g., deforestation promotes wildfires at forest edges, which leads to greenhouse gas emissions that further increase global warming[21] – and thus likely underestimate the potential for critical forest transitions. Other studies consider these interactions by assessing the combined impact of land-use change and climate change, but do not explicitly separate their individual contributions[17,22]. This means that forest changes and transitions cannot be directly linked to deforestation and/or global warming levels, which is necessary for a holistic understanding of the risk of large-scale forest transitions in the future.

Although several studies suggest that a large-scale transition to savanna vegetation in the Amazon might occur gradually over several decades[15,23], an assessment of the local patterns of abrupt versus gradual forest changes across the Amazon basin in response to land-use change and climate change is currently lacking. However, such an assessment is crucial, since an increasing frequency of local abrupt tree mortality and forest transitions could be an early signal of a declining resilience of the ecosystem, manifesting in a reduced capacity of the forest to withstand and recover from disturbances[24–28]. Uncovering these early signals is crucial, since they indicate an increasing risk of a large-scale transition of the Amazon rainforest, which could reinforce global warming to an extent that could hamper the goals of the Paris Agreement[29,30], posing a severe threat to global socio-ecological well-being[15].

Here, we provide a holistic assessment of Amazon forest vulnerability to individual and combined pressures of land-use change and climate change in the past and under different future pathways. We leverage data from four state-of-the-art Earth System Models (ESMs) to assess spatial and temporal trajectories of forest decline, which we define as reductions in tree cover with or without a 'structural' transition, i.e., forest transitions to a different vegetation regime (e.g., savanna). We address critical gaps in existing studies by 1) disentangling the contribution of each driver to forest decline, while still accounting for their interactions and 2) uncovering abrupt forest decline as early indications of declining resilience. This enables us to identify spatial hotspots of

forest vulnerability and to attribute non-linear and abrupt decline to specific levels of deforestation and/or global warming to assess the plausibility of a potentially imminent large-scale structural forest transition. Important terms and their definitions are provided in Tab. 1.

Results

Overview

We use data from the 6th phase of the Coupled Model Intercomparison Project (CMIP6)[31], including ESMs that simulate dynamic vegetation. Models without dynamic vegetation were excluded, as they do not simulate structural transitions from forest to an alternative vegetation regime[28] with changing climate and/or natural disturbances. The chosen models rely on different land components to simulate the response of vegetation to land-use and changing environmental conditions and therefore differ in their (degree of) implementation of anthropogenic and natural disturbances and vegetation demography (Tab. 2). This allows us to sample a range of model uncertainties related to these processes.

Our methodology includes several steps that are applied to the historical (1950-2014) and future (2015-2100) periods separately (Fig. 1): First, we detect for each model local 'forest declines', defined as any long-term decrease in tree cover fraction in a specific grid cell. Forest decline may or may not imply that a structural transition from forest to another vegetation regime happens. To identify forest declines involving a structural transition, we apply model-specific tree cover thresholds (see Supporting Information). By definition, including structural transitions in the calculation of forest area changes will introduce more sudden changes compared to only considering tree cover changes. This helps to identify spatial 'hotspots' of severe forest damage and vulnerability and facilitates the comparison of historical forest dynamics in ESMs with observational datasets, which typically only capture structural forest transitions. Second, we assess the timescales over which forest declines happen, by classifying the annual rate of forest decline as either abrupt or gradual. This step is crucial, as an increasing frequency of non-linear and abrupt forest declines indicate a loss of forest resilience and an increased risk of structural transitions[4,24,25]. Third, we identify the main driver of forest decline, which is either anthropogenic climate change or land-use change. There is no a priori separation of the main driver of forest decline in the model output. To ensure a robust attribution of forest decline to each driver, we develop two different approaches. This is done by choosing a threshold for the carbon emissions from land-use change (=fLuc), which serves as a proxy for the degree of land-use activity in each grid cell. If the fLuc threshold is exceeded, forest decline is attributed to land-use change. If fLuc is not exceeded and the likelihood of natural climate variability being the driver of forest decline is very low, forest decline is attributed to climate change. At each grid cell we differentiate between 1) local forest decline imposed by local land-use change (primarily through deforestation) and 2) local forest decline due to climate change, including impacts of radiative forcing as well as impacts of remote land-use change imposed in other grid cells (see Supporting Information). For the future period from 2015 until 2100, we consider the SSP3-7.0 and the SSP5-8.5 scenarios, which assume a high degree of future land-use change (especially deforestation) and a fossil-fuel based economy, respectively (see Supporting Information)[32]. For our data analysis, we further aggregate local forest decline to basin-wide forest decline to demonstrate the vulnerability of the whole Amazon ecosystem to different degrees of deforestation and global warming.

Basin-wide dynamics of forest decline

We analyze how much forest has declined historically due to land-use change and climate change in the Amazon basin and how much forest is projected to additionally decline until 2100 under SSP3-7.0 and SSP5-8.5 (Fig. 2). The basin-wide area of forest decline is calculated by summing the local (i.e., grid-cell) area of forest decline over the whole Amazon basin. This allows us to assess how resilient the forest has been on an ecosystem scale rather than at the local scale and whether there is a danger of basin-wide structural forest transition under unabated global warming and deforestation. We further dissect overall forest decline into areas with and without structural transition (from forest to other vegetation types). This additional layer of

information is provided for all models except for GFDL-ESM4, as we could not robustly quantify an optimum tree cover threshold for this model due to strong differences between the simulated historical forest area change and the Land-Use Harmonization 2 dataset (LUH2)[33] forcing dataset. Over the entire historical period from 1950 to 2014, we find that, averaged across the four employed ESMs, forest declined over an area of 0.8 (model range: 0.2-1.2) mio. km^2, corresponding to 14% (7-19%) of the initial (1950) forest area. Our attribution reveals that 0.6 (0.2-0.9) mio. km^2 of forest declined due to land-use change and 0.2 (0.0-0.3) mio. km^2 due to climate change (Fig. 2). Around 86% (79-96%) of the total historical forest decline in the Amazon basin is made up by areas with a structural transition (i.e., transition from forest to other vegetation types), whereas the remaining 14% is explained by areas without a structural forest transition (i.e., forest remains forest).

We compare the historical area of forest decline with structural forest transitions due to land-use change simulated by three ESMs (EC-Earth3-Veg, MPI-ESM1-2-LR, UKESM1-0-LL) to an observational dataset (MapBiomas[34]). To facilitate a direct comparison between the ESMs and the observational dataset, we choose the period of the observational data (1985-2014) and only consider the grid cells where a structural transition from forest to other vegetation happens. The comparison shows that the model mean (319,094 km^2) is smaller than the observational dataset (MapBiomas: 497,802 km^2). However, there is a large range across the models (140,930-437,000 km^2), which is partly related to the different initial spatial distribution of forest at the start of the historical period (Fig. S1). Consequently, differences across the models are reduced when expressing the area of structural forest transition as a fraction of the forest area at the start of the observational record in 1985 (Tab. 3). Accordingly, all models underestimate the historical fraction of structural forest transition, slightly (MPI-ESM1-2-LR and UKESM1-0-LL) and strongly (EC-Earth3-Veg), respectively. We further compare the spatial pattern of the historical structural forest transitions between the ESMs and the observational dataset (Fig. S2). This reveals that all models capture the general pattern with hotspots of land-use change induced structural forest transitions in the Southeast of the basin. However, all models show a sparser pattern of structural forest transitions compared to the observations, indicating that the land-use forcing underestimates the spatial density of deforestation. To investigate whether the spatial resolution of the ESMs might also partly explain the differences to the MapBiomas data, we lower the spatial resolution of the MapBiomas data from its native resolution of 30m to the ESM resolution of 100km. This shows that especially areas where structural forest transitions are sparse are not captured at the lower spatial resolution. This occurs because local-scale, sparse transitions within the large area of a grid cell at the coarse resolution may not sufficiently decrease the overall tree cover fraction of the grid cell to be detected as a forest transition. Therefore, we conclude that - apart from the forcing dataset and the initial forest distribution - the spatial resolution is a major driver for differences between the ESMs and the observations.

Under the assumption that the historical deforestation rates of the past 30 years largely persist into the future (SSP3-7.0), around 0.7 (0.4-1.1) mio. km^2 of forest are projected to additionally decline by 2100 due to land-use change (Fig. 2). On the other hand, following a path of marginal deforestation until 2030 and no deforestation afterwards (SSP5-8.5), only 0.2 (0.0-0.3) mio. km^2 of forest are projected to decline by 2100. Reaching a global warming level of around 5°C by 2100 (SSP3-7.0), around 0.3 (0.1-0.5) mio. km^2 of forest are projected to decline due to climate change. Reaching an even higher global warming level of 6°C by 2100 (SSP5-8.5), forest decline due to climate change further increases to 0.5 (0.1-0.9) mio. km^2. Around 77% (39-98%) and 65% (12-99%) of future forest decline includes a structural forest transition under SSP3-7.0 and SSP5-8.5, respectively. Overall, land-use change is projected to reduce the initial (1950) forest area by around 25% (17-37%) until 2100 under continued deforestation (SSP3-7.0). Moreover, unabated climate change is projected to reduce the historical forest area by around 9% (2-13%) under SSP3-7.0 to 13% (4-20%) under SSP5-8.5.

Although continued deforestation is projected to cause a larger forest area decline compared to climate change, we find a non-linear increase in the forest decline area due to climate change. This dynamic is consistent across all models and both scenarios (Fig. 3). We use a breakpoint detection approach (see Methods) to show that the intensification of the impact of climate change starts at around 2073 (2069-2079) in SSP3-7.0 and around 2063 (2058-2066) in SSP5-8.5. This corresponds to a global warming level of around 3.6°C (2.9-4.6°C) (SSP3-7.0) and 3.5°C (2.3-

4.6°C) (SSP5-8.5) (Tab. 2). As a result of the rapidly advancing negative impacts of climate change on the forest, compared to 1950-1980, the rate of forest decline over 2070-2100 increases by a factor of 6 (1-11) (SSP3-7.0) and 8 (2-16) (SSP5-8.5).

We further assess the fraction of the forest area decline that is characterized by abrupt and gradual change, respectively (Fig. 4). This serves to assess whether there is an increasing risk of abrupt change under continued climate change and land-use change, which would indicate that the forest ecosystem is lacking resilience to withstand the degree of disturbance and is in danger of a large-scale irreversible structural transition. Between 1950 and 2100, there is a higher share of gradual forest decline (SSP3-7.0: 58-98%, SSP5-8.5: 32-100%) than abrupt forest decline (SSP3-7.0: 2-42%, SSP5-8.5: 0-68%). Evaluating the models in terms of the degree of detail in their implementation of forest demography and the most important disturbance processes (Tab. 2) indicates to which degree models are expected to capture the impact of species competition, climate change and other environmental changes on forests[35]. Two of the models used in this study (EC-Earth3-Veg and GFDL-ESM4) can be considered more comprehensive in their land components compared to the other two models (UKESM1-0-LL and MPI-ESM1-2-LR), since they include competition, disturbances and mortality across different age-height cohorts[28,36,37]. This enables EC-Earth3-Veg and GFDL-ESM4 to simulate the spatial heterogeneity of the impact of climatic changes and disturbances at a higher degree of detail compared to the other two models[31]. The two models with more comprehensive land components stand out in several aspects (Fig. 4). First, they simulate a much higher fraction of abrupt forest decline (SSP3-7.0: 37-42%, SSP5-8.5: 42-68%), compared to the other two models (SSP3-7.0: 2-5%, SSP5-8.5: 0-2%). Second, they simulate that the highest share of abrupt decline across both scenarios and drivers occurs under SSP5-8.5 due to climate change (36-63%). Third, they simulate a consistent increase in the share of abrupt forest decline with increasing climate change over the whole future period (SSP5-8.5) and towards the end of the 21st century (under SSP3-7.0), respectively.

Local dynamics of forest decline

We analyze how intensities, rates and timing of forest decline per driver vary spatially across the Amazon basin (Fig. 5). This allows us to identify emerging hotspots of forest vulnerability and early indications of declining resilience to climate change and land-use change.

Land-use change leads to high-intensity (>40% decline relative to the 1950 forest area) forest decline on a larger scale, triggering structural transitions from forest to other vegetation types. Climate change mainly leads to low (<20%) to medium intensity (>20-<40%) local forest decline and does not trigger structural forest transitions on a larger scale. This is at least partly explained by the fact that forest decline due to climate change intensifies only in the second half of the 21st century, while forest decline due to land-use change starts earlier (Fig. 5c).

Consistent across all models (Fig. 5b, Fig. S3), land-use change generally leads to local forest decline in the south and southeast of the Amazon basin under historical conditions (Fig. 5c), which agrees well with the observations[34,38]. Under the SSP3-7.0 scenario, land-use change causes large-scale forest decline with a structural transition in the west of the basin with the largest impact from ca. 2040 onwards. Under the SSP5-8.5 scenario, there is only a marginal additional local forest decline due to land-use change until 2100. Consistent across all models, climate change leads to local forest decline in the central Amazon under both SSPs and stretches west under SSP5-8.5 (Fig. 5b), with the largest impact between 2070 and 2100 (Fig. 5c).

Discussion

We show that, basin-wide, land-use change will remain the major driver of forest decline under ongoing future deforestation, reducing the 1950 forest extent by up to 25% until 2100. This would imply reaching the critical deforestation threshold range of 20-25% suggested by Nobre et al.[17], in which a potentially irreversible large-scale structural transition of the forest to a degraded state is risked. Our results show that such a basin-wide transition is unlikely to happen within the 21st century, even under high degrees of global warming. This is in general agreement with other recent studies[19,22]. However, we unveil a breakpoint reached around the middle of the century, at an earliest global warming level of 2.3°C. Beyond this breakpoint, all models project that the rate of forest decline due to climate change increases non-linearly – by a factor of up to 16 over 2070-2100 compared to 1950-1980. Along with this non-linear increase, we find that the two models with the most comprehensive land components project an increase in the share of abrupt forest decline attributed to climate change. These findings highlight a decreasing capacity of the Amazon rainforest to withstand climatic changes, indicating a declining resilience of the ecosystem with progressing climate change[4,24,28]. We find that the regions that are most vulnerable to forest decline in response to global warming are the currently intact forests of central, northern (under both pathways) and western (under SSP5-8.5) Amazon. This is critical, as an increased mortality of these forests could lead to devastating socio-ecological consequences, since they host an exceptionally high diversity of plant and animal species[12,39] and belong to numerous indigenous territories[40] and protected areas[41]. Apart from these local impacts, widespread structural forest transitions in the central and northern Amazon are projected to have far-reaching negative impacts on water supply in the western Amazonian countries[4,42,43] and further downstream[16], increasing the risk of an ecosystem-scale structural transition[24].

While ESMs are a unique tool for projecting future ecosystem states, key uncertainties persist in their simulated vegetation responses to different types of disturbances, water and nutrient limitations and to enhanced levels of CO_2 ("CO_2 fertilization" or "CO_2 effect")[28,44–49]. These uncertainties partly root in incomplete representations of disturbance processes (e.g., logging and fires), mortality and post-disturbance recovery as well as species composition and forest demography[44]. A substantial gap persists between observations and models[50] in the Amazon, where the former suggest that substantial parts of the forest are already experiencing potentially irreparable damage and transitions to alternative vegetation regimes[4,6,7,14,51], whereas the latter tend to simulate a high forest resilience even under high degrees of global warming[4,51]. This is partly explained by the fact that many ESMs do not capture the observed saturation and decline of the carbon sink in intact forests[45,52], likely due to an underestimation of tree mortality in response to natural disturbance[45]. Furthermore, ESMs exhibit uncertainties in their representation of the Amazonian hydrological cycle. Specifically, some ESMs underestimate seasonal precipitation recycling – partly due to an underestimation of evapotranspiration[53] – and use simplified assumptions on the relationship between transpiration and precipitation[54]. Recent research suggests that direct negative physiological effects on plants, such as reduced transpiration caused by deforestation, drought or rising CO_2 can lead to large-scale decreases in precipitation, which challenges ecosystem resilience[4,55,56]. Many models do not fully incorporate these physiological effects on plants and therefore likely overestimate forest resilience[4,15,51]. However, recent studies demonstrate that models with more detailed plant hydraulics or drought-induced leaf shedding are able to better reproduce observed carbon losses and canopy-level responses to drought, indicating a promising path forward[28,57,58]. Despite the mentioned limitations, ESMs have a clear advantage over observational data[59] in that they allow for clearly isolating the vegetation response to specific natural, indirect anthropogenic (e.g., increasing atmospheric CO_2) and direct anthropogenic drivers (e.g., land-use change)[60]. Consequently, they are an indispensable tool for deepening our understanding of non-linear ecosystem transitions in response to specific drivers and thresholds. We deliberately include ESMs with varying degrees of detail in their land components in our analysis to demonstrate that improving model representations of forest demography and disturbance processes will also enable them to predict structural transitions and signs of decreasing forest resilience to a larger degree. This finding is crucial, as it addresses the existing gap between observations and models in the Amazon[50] and supports that a promising path forward to bridging this gap involves improved model

representations of forest mortality and natural disturbance processes as well as a stronger integration of process-based modeling and observations[51,61].

Recent studies with fully-coupled ESMs either only focus on climate change impacts on forest stability in idealized CO_2 forcing simulations[19] or use plausible future pathways, but do not disentangle climate change impacts from land-use change impacts[17,22]. Moreover, indicators of decreasing forest resilience as early signs of imminent large-scale structural transitions, such as the occurrence of local abrupt forest decline, remain largely unexplored. Our unique detection and attribution framework enables us to address these critical knowledge gaps by uncovering the spatiotemporal patterns of forest decline due to individual and combined pressures of climate change and land-use change. We further unravel early indications of declining forest resilience by analyzing the occurrence of abrupt forest decline on the local scale as well as non-linearities in the response of the forest to ongoing global warming on the basin scale. This holistic approach provides a detailed and robust assessment of the vulnerability of the Amazon rainforest to different anthropogenic stressors, which is the base for shaping effective policy measures. Our results emphasize that, by only considering impacts of climate change and neglecting land-use change, the primary driver of forest decline and structural transitions in the Amazon is overlooked, leading to a substantial overestimation of the stability of the Amazon ecosystem. The non-linear increase in abrupt forest decline at a minimum global warming level of 2.3°C suggests that the resilience of the Amazon forest is diminishing and that a large-scale structural transition towards a degraded ecosystem is likely if no strong countermeasures are taken. This finding is particularly concerning, as current trajectories are projected to result in a global warming of 2.5°C-2.9°C by 2100. This reinforces the urgent need for increased efforts to reduce deforestation and forest degradation through forest protection, conservation and sustainable land-use practices and for climate mitigation in line with the Paris Agreement.

Materials and Methods

Detection of local forest decline and its characteristic timescales

We detect local (i.e., grid cell level) forest decline with and without structural transition from forest to other vegetation types in the Amazon.

First, we calculate the annual change in tree cover fraction at each grid cell over the historical (1950-2014) and future time periods (2015-2100). The periods are treated separately since the CO_2 and land-use change forcings are based on different assumptions (see Supporting Information). The starting point of a local forest decline marks the first time step in the time series of annual change in tree cover fraction that fulfills the following conditions: 1) the change in tree cover fraction must be negative (i.e., the forest is declining). To filter out grid cells where forest declines initially, but recovers afterwards, we further apply the condition that the average annual change in tree cover fraction of all subsequent timesteps is negative (i.e., forest decline continues until the end of the respective time period). 2) it must be highly unlikely that the forest decline would occur under natural climate variability. Building on the approaches by Drijfhout et al.[22] and Smith et al.[62], the average annual change in tree cover fraction (from the start of the event until the end of the respective period) must be smaller than the 5^{th} percentile of the annual changes in the piControl simulation. We repeat the two previous steps for different degrees of smoothing of the initial time series of tree cover fraction. This step is necessary to filter out short-term climate variability, as we are only interested in the long-term trend of forest decline. We smooth the initial time series (prior to applying conditions 1-2) by applying a Savitzky-Golay filter[63] over a 15-year and 30-year time window, respectively and compare the resulting classification to the results when no smoothing filter is applied to account for uncertainties related to this assumption. We subsequently only consider local forest decline that occurs in at least two out of the three smoothing options (i.e., 15-year, 30-year, no smoothing). For models with multiple ensemble members (all except for GFDL-ESM4), we additionally quantify the signal-to-noise ratio (i.e., the ensemble mean divided by the ensemble standard deviation[64] of the occurrence of forest decline per member (0=no forest decline, 1=forest decline) to estimate the magnitude of the forced climate signal (the ensemble mean) in relation to the internal climate variability (the ensemble standard deviation). Accordingly, if more than half of the ensemble members simulate forest

decline at a specific grid cell, the signal-to-noise ratio exceeds 1, which means that the forced climate change signal exceeds the internal variability[64]. This serves as an additional criterion (to the piControl criterion) to ensure that the local forest decline is caused by anthropogenic changes (either land-use change or climate change) and not internal variability.

We assess the timescales over which local forest decline happens by classifying the annual rate of tree cover change during the time period of forest decline as either abrupt or gradual. We follow the approach by Berdugo et al.[27], where different types of models that represent gradual (linear and quadratic models) or abrupt (step model) behaviour are fitted to the annual time series of local forest decline. The type of change is classified according to the group of models (abrupt or gradual) that fit best to each time series of forest decline, i.e., the model with the smallest Akaike Information Critera (AIC) value. The purpose of this analysis is to analyze whether the annual rates of forest decline become increasingly abrupt beyond a specific deforestation and/or global warming level, which indicates an increased risk for upcoming structural forest transitions. Consequently, the annual fractions of abrupt versus gradual basin-wide forest decline per driver (Fig. 4) only include grid cells that have not yet experienced structural forest transitions.

Attribution of local forest decline to climate change and land-use change

The underlying assumption for attributing local forest decline to land-use change or climate change is that the degree of land-use change can be traced back through the carbon emissions from land-use change (fLuc) (=instantaneous fluxes from land-use change to the atmosphere) that are simulated by each model. It is not a priori known which threshold for fLuc leads to the most accurate attribution of forest decline to land-use change. Therefore, we calculate a range of percentiles (80 to 100 in 1 percentile steps) for fLuc. The percentiles are calculated for each ESM from the fLuc data of all grid cells within the Amazon basin, all scenarios (SSP3-7.0 and SSP5-8.5) and all periods (historical and future). The optimum threshold is then chosen according to two approaches. The first approach compares 1) the simulated total area of forest cover change across the Amazon region attributed to land-use change, derived from applying the respective fLuc percentile threshold with 2) the forced total area of forest change across the Amazon region from the LUH2 dataset that each model was forced with (Fig. S4 'Attribution approach 1'). The LUH2 dataset only includes forest changes due to land-use change, making it suitable to evaluate whether our attribution of the simulated forest changes to land-use change in the ESMs is accurate. Consequently, we choose the percentile value for fLuc that leads to the highest agreement, measured by the highest Pearson correlation coefficient, between 1) and 2). The second approach (Fig. S4 'Attribution approach 2') compares 1) the annual sum of land-use related emissions across the Amazon region (i.e., spatial integral over fLuc) with 2) the simulated annual sum of grid cells with forest decline attributed to land-use change across the Amazon region. This approach is based on the assumption that the occurrence of grid cells with forest decline increases (decreases) with increasing (decreasing) basin-wide fLuc. Consequently, if the fLuc percentile threshold is chosen too low (high), too many (few) grid cells with forest decline will be attributed to land-use change, manifesting in a higher disagreement (i.e., lower Pearson correlation coefficient) between 1) and 2).

Overall, there is a high consistency (model range across both pathways: 74-95%, calculated as % of grid cells with the same driver across both attribution approaches) in the resulting attribution of forest decline to land-use change between both attribution approaches (Fig. S5), indicating a robust attribution. To account for the remaining small uncertainties related to the choice of attribution approach, we use the average of both attribution approaches in all of our results.

Intensification of basin-wide forest decline due to climate change

We calculate the timing and the corresponding global warming level at which the basin-wide forest decline attributed to climate change intensifies non-linearly.

We use the the PiecewiseLinFit function from the pwlf package[65] in python, which automatically finds breakpoints in a time series (here: basin-wide forest decline, see Fig. 3) according to a specified number of segments (here: 2) by minimizing the sum-of-squares error of the residuals. The approach to detect abrupt shifts via a piecewise linear regression has been shown to work

particularly well in previous applications[66–68]. The global warming level at the timing of the breakpoint (Tab. 2) is subsequently calculated by combining information from the SSP3-7.0 and SSP5-8.5 scenarios and the 1pctCO2 simulation. We quantify the atmospheric greenhouse gas concentration at the timing of the breakpoint from the greenhouse gas forcing of the SSPs. The simulated global warming level at the respective breakpoint in the SSP simulations will include biogeophysical effects from land-use change (e.g., warming due to deforestation[59]). However, we want to know at which global warming level the non-linear forest decline due to climate change starts, excluding any land-use effects. Therefore, we derive the global warming level from the simulated air temperature of the 1pctCO2 simulation, where only CO_2 is increased by 1% per year without any land-use changes[31]. We quantify the global warming level at the CO_2 concentration in the 1pctCO2 simulation that is the closest to the CO_2 concentration in the SSP simulations at the respective breakpoint.

Use of generative AI and AI-assisted technologies in the writing process

During the preparation of this work, the authors used ChatGPT (GPT-5) and Google NotebookLM to improve language and grammar. After using these tools, the authors reviewed and edited the content as needed and take full responsibility for the content of the publication.

Data, Materials, and Software Availability

All CMIP6 data used in our analysis can be retrieved from the Earth System Grid Federation (ESGF; https://esgf-metagrid.cloud.dkrz.de). The codes used for the detection and attribution, analysis and production of figures are available at: (repository will be provided upon acceptance).

Acknowledgments

This work was supported by the German Stifterverband für die Deutsche Wissenschaft e.V. in collaboration with Volkswagen AG (Addressing the new role of terrestrial CO2 fluxes for climate mitigation). This work used resources of the Deutsches Klimarechenzentrum (DKRZ) granted by its Scientific Steering Committee (WLA) under Project ID bm1240. This is ClimTip contribution \#39; the ClimTip project has received funding from the European Union's Horizon Europe research and innovation programme under grant agreement No. 101137601. N.B. acknowledges further funding by the Volkswagen foundation and by the European Union’s Horizon 2020 research and innovation programme under the Marie Sklodowska-Curie grant agreement No.956170.

References

1. Rosan, T. M. *et al.* Synthesis of the land carbon fluxes of the Amazon region between 2010 and 2020. *Commun. Earth Environ.* **5**, 46 (2024).
2. Friedlingstein, P. *et al.* Global Carbon Budget 2023. *Earth Syst. Sci. Data* **15**, 5301–5369 (2023).
3. Bochow, N. & Boers, N. The South American monsoon approaches a critical transition in response to deforestation. *Sci. Adv.* **9**, eadd9973 (2023).
4. Flores, B. M. *et al.* Critical transitions in the Amazon forest system. *Nature* **626**, 555–564 (2024).
5. Eltahir, E. A. B. & Bras, R. L. Precipitation recycling in the Amazon basin. *Q. J. R. Meteorol. Soc.* **120**, 861–880 (1994).
6. Boulton, C. A., Lenton, T. M. & Boers, N. Pronounced loss of Amazon rainforest resilience since the early 2000s. *Nature Climate Change* vol. 12 271–278 (2022).
7. Gatti, L. V. *et al.* Amazonia as a carbon source linked to deforestation and climate change. *Nature* **595**, 388–393 (2021).
8. Lapola, D. M. *et al.* The drivers and impacts of Amazon forest degradation. *Science* vol. 379 eabp8622 (2023).
9. Marengo, J. A. *et al.* Changes in Climate and Land-use Over the Amazon Region: Current and Future Variability and Trends. *Frontiers in Earth Science* vol. 6 (2018).
10. Hirota, M., Holmgren, M., Van Nes, E. H. & Scheffer, M. Global Resilience of Tropical Forest and Savanna to Critical Transitions. *Science* **334**, 232–235 (2011).
11. Lovejoy, T. E. & Nobre, C. Amazon Tipping Point. *Sci Adv* vol. 4 eaat2340 (2018).
12. Nobre, C. & Encalada, A. Amazon Assessment Report 2021. (2021) doi:10.55161/rwsx6527.
13. Staal, A. *et al.* Hysteresis of tropical forests in the 21st century. *Nat Commun* vol. 11 4978 (2020).
14. Wunderling, N. *et al.* Recurrent droughts increase risk of cascading tipping events by outpacing adaptive capacities in the Amazon rainforest. *Proc Natl Acad Sci U S A* vol. 119 e2120777119 (2022).
15. Armstrong McKay, D. I. *et al.* Exceeding 1.5 degrees C global warming could trigger multiple climate tipping points. *Science* vol. 377 eabn7950 (2022).
16. Boers, N., Marwan, N., Barbosa, H. M. J. & Kurths, J. A deforestation-induced tipping point for the South American monsoon system. *Sci. Rep.* **7**, 41489 (2017).
17. Nobre, C. A. *et al.* Land-use and climate change risks in the Amazon and the need of a novel sustainable development paradigm. *Proc Natl Acad Sci U S A* vol. 113 10759–68 (2016).
18. Nian, D. *et al.* A potential collapse of the Atlantic Meridional Overturning Circulation may stabilise eastern Amazonian rainforests. *Communications Earth & Environment* vol. 4 (2023).
19. Parry, I. M., Ritchie, P. D. L. & Cox, P. M. Evidence of localised Amazon rainforest dieback in CMIP6 models. *Earth Syst. Dyn.* **13**, 1667–1675 (2022).
20. Spracklen, D. V. & Garcia- Carreras, L. The impact of Amazonian deforestation on Amazon basin rainfall. *Geophys. Res. Lett.* **42**, 9546–9552 (2015).
21. Brando, P. M. *et al.* The gathering firestorm in southern Amazonia. *Sci. Adv.* **6**, eaay1632 (2020).
22. Drijfhout, S. *et al.* Catalogue of abrupt shifts in Intergovernmental Panel on Climate Change climate models. *Proc Natl Acad Sci U S A* vol. 112 E5777-86 (2015).
23. Lenton, T. M. *et al.* Tipping elements in the Earth's climate system. *Proc. Natl. Acad. Sci.* **105**, 1786–1793 (2008).
24. Forzieri, G., Dakos, V., McDowell, N. G., Ramdane, A. & Cescatti, A. Emerging signals of declining forest resilience under climate change. *Nature* **608**, 534–539 (2022).
25. Ratajczak, Z. *et al.* Abrupt Change in Ecological Systems: Inference and Diagnosis. *Trends Ecol. Evol.* **33**, 513–526 (2018).
26. Liu, Y., Kumar, M., Katul, G. G. & Porporato, A. Reduced resilience as an early warning signal of forest mortality. *Nat. Clim. Change* **9**, 880–885 (2019).

27. Berdugo, M., Gaitan, J. J., Delgado-Baquerizo, M., Crowther, T. W. & Dakos, V. Prevalence and drivers of abrupt vegetation shifts in global drylands. *Proc Natl Acad Sci U S A* vol. 119 e2123393119 (2022).
28. Cano, I. M. *et al.* Abrupt loss and uncertain recovery from fires of Amazon forests under low climate mitigation scenarios. *Proc. Natl. Acad. Sci.* **119**, e2203200119 (2022).
29. Bathiany, S., Claussen, M., Brovkin, V., Raddatz, T. & Gayler, V. Combined biogeophysical and biogeochemical effects of large-scale forest cover changes in the MPI earth system model. *Biogeosciences* **7**, 1383–1399 (2010).
30. Malhi, Y. *et al.* The regional variation of aboveground live biomass in old-growth Amazonian forests. *Glob. Change Biol.* **12**, 1107–1138 (2006).
31. Eyring, V. *et al.* Overview of the Coupled Model Intercomparison Project Phase 6 (CMIP6) experimental design and organization. *Geoscientific Model Development* vol. 9 1937–1958 (2016).
32. O'Neill, B. C. *et al.* The Scenario Model Intercomparison Project (ScenarioMIP) for CMIP6. *Geoscientific Model Development* vol. 9 3461–3482 (2016).
33. Hurtt, G. C. *et al.* Harmonization of global land-use change and management for the period 850–2100 (LUH2) for CMIP6. *Geoscientific Model Development* vol. 13 5425–5464 (2020).
34. Souza, C. M. *et al.* Reconstructing Three Decades of Land-use and Land Cover Changes in Brazilian Biomes with Landsat Archive and Earth Engine. *Remote Sens.* **12**, 2735 (2020).
35. McDowell, N. G. *et al.* Pervasive shifts in forest dynamics in a changing world. *Science* **368**, eaaz9463 (2020).
36. Forrest, M., Tost, H., Lelieveld, J. & Hickler, T. Including vegetation dynamics in an atmospheric chemistry-enabled general circulation model: linking LPJ-GUESS (v4.0) with the EMAC modelling system (v2.53). *Geosci. Model Dev.* **13**, 1285–1309 (2020).
37. Shevliakova, E. *et al.* The Land Component LM4.1 of the GFDL Earth System Model ESM4.1: Model Description and Characteristics of Land Surface Climate and Carbon Cycling in the Historical Simulation. *J. Adv. Model. Earth Syst.* **16**, e2023MS003922 (2024).
38. F. G. Assis, L. F. *et al.* TerraBrasilis: A Spatial Data Analytics Infrastructure for Large-Scale Thematic Mapping. *ISPRS Int. J. Geo-Inf.* **8**, 513 (2019).
39. Ter Steege, H. *et al.* Mapping density, diversity and species-richness of the Amazon tree flora. *Commun. Biol.* **6**, 1130 (2023).
40. Red Amazónica de Información Socioambiental Georreferenciada (RAISG). Indigenous Territories. (2023).
41. Red Amazónica de Información Socioambiental Georreferenciada (RAISG). Natural Protected Areas. (2023).
42. De Vasconcelos, A. C. F. *et al.* Land-use dynamics in Brazilian La Plata Basin and anthropogenic climate change. *Clim. Change* **127**, 73–81 (2014).
43. Weng, W., Luedeke, M. K. B., Zemp, D. C., Lakes, T. & Kropp, J. P. Aerial and surface rivers: downwind impacts on water availability from land-use changes in Amazonia. *Hydrology and Earth System Sciences* vol. 22 911–927 (2018).
44. Fisher, R. A. *et al.* Vegetation demographics in Earth System Models: A review of progress and priorities. *Glob. Change Biol.* **24**, 35–54 (2018).
45. Koch, A., Hubau, W. & Lewis, S. L. Earth System Models Are Not Capturing Present-Day Tropical Forest Carbon Dynamics. *Earths Future* **9**, e2020EF001874 (2021).
46. Chen, C., Riley, W. J., Prentice, I. C. & Keenan, T. F. CO_2 fertilization of terrestrial photosynthesis inferred from site to global scales. *Proc. Natl. Acad. Sci.* **119**, e2115627119 (2022).
47. Hofhansl, F. *et al.* Amazon Forest Ecosystem Responses to Elevated Atmospheric CO2 and Alterations in Nutrient Availability: Filling the Gaps with Model-Experiment Integration. *Front. Earth Sci.* **4**, (2016).
48. Terrer, C. *et al.* Nitrogen and phosphorus constrain the CO2 fertilization of global plant biomass. *Nat. Clim. Change* **9**, 684–689 (2019).
49. Walker, A. P. *et al.* Integrating the evidence for a terrestrial carbon sink caused by increasing atmospheric CO_2. *New Phytol.* **229**, 2413–2445 (2021).
50. Huntingford, C. *et al.* Simulated resilience of tropical rainforests to CO2-induced climate change. *Nat. Geosci.* **6**, 268–273 (2013).

589 51. Lenton, T. M. *et al.* Remotely sensing potential climate change tipping points across
590 scales. *Nat. Commun.* **15**, 343 (2024).
591 52. Hubau, W. *et al.* Asynchronous carbon sink saturation in African and Amazonian tropical
592 forests. *Nature* **579**, 80–87 (2020).
593 53. Baker, J. C. A. & Spracklen, D. V. Divergent Representation of Precipitation Recycling in
594 the Amazon and the Congo in CMIP6 Models. *Geophysical Research Letters* vol. 49 (2022).
595 54. Baudena, M., Tuinenburg, O. A., Ferdinand, P. A. & Staal, A. Effects of land-use change
596 in the Amazon on precipitation are likely underestimated. *Glob. Change Biol.* **27**, 5580–5587
597 (2021).
598 55. Lapola, D. M. *et al.* Not just semantics: CO_2 fertilization can be a disturbance leading to
599 worldwide forest degradation. *PLANTS PEOPLE PLANET* **7**, 638–643 (2025).
600 56. Sampaio, G. *et al.* CO_2 physiological effect can cause rainfall decrease as strong as
601 large-scale deforestation in the Amazon. *Biogeosciences* **18**, 2511–2525 (2021).
602 57. Wey, H., Pongratz, J., Nabel, J. E. M. S. & Naudts, K. Effects of Increased Drought in
603 Amazon Forests Under Climate Change: Separating the Roles of Canopy Responses and Soil
604 Moisture. *J. Geophys. Res. Biogeosciences* **127**, e2021JG006525 (2022).
605 58. Papastefanou, P. *et al.* Recent extreme drought events in the Amazon rainforest:
606 assessment of different precipitation and evapotranspiration datasets and drought indicators.
607 *Biogeosciences* vol. 19 3843–3861 (2022).
608 59. Pongratz, J. *et al.* Land-use Effects on Climate: Current State, Recent Progress, and
609 Emerging Topics. *Current Climate Change Reports* (2021) doi:10.1007/s40641-021-00178-y.
610 60. O'Sullivan, M. *et al.* Process-oriented analysis of dominant sources of uncertainty in the
611 land carbon sink. *Nat. Commun.* **13**, 4781 (2022).
612 61. Au, J. *et al.* Forest productivity recovery or collapse? Model-data integration insights on
613 drought-induced tipping points. *Glob. Change Biol.* **29**, 5652–5665 (2023).
614 62. Smith, T., Traxl, D. & Boers, N. Empirical evidence for recent global shifts in vegetation
615 resilience. *Nature Climate Change* (2022) doi:10.1038/s41558-022-01352-2.
616 63. Savitzky, Abraham. & Golay, M. J. E. Smoothing and Differentiation of Data by Simplified
617 Least Squares Procedures. *Anal. Chem.* **36**, 1627–1639 (1964).
618 64. Deser, C. & Phillips, A. S. A range of outcomes: the combined effects of internal
619 variability and anthropogenic forcing on regional climate trends over Europe. *Nonlinear Process.*
620 *Geophys.* **30**, 63–84 (2023).
621 65. Jekel, C. & Venter, G. pwlf: A Python Library for Fitting 1D Continuous Piecewise Linear
622 Functions. (2019).
623 66. Bathiany, S., Hidding, J. & Scheffer, M. Edge Detection Reveals Abrupt and Extreme
624 Climate Events. *J. Clim.* **33**, 6399–6421 (2020).
625 67. Mudelsee, M. Ramp function regression: a tool for quantifying climate transitions.
626 *Comput. Geosci.* **26**, 293–307 (2000).
627 68. Riechers, K. & Boers, N. Significance of uncertain phasing between the onsets of stadial–
628 interstadial transitions in different Greenland ice core proxies. *Clim. Past* **17**, 1751–1775 (2021).
629 69. Ibáñez, I. *et al.* Forest resilience under global environmental change: Do we have the
630 information we need? A systematic review. *PLOS ONE* **14**, e0222207 (2019).
631 70. Döscher, R. *et al.* The EC-Earth3 Earth system model for the Coupled Model
632 Intercomparison Project 6. *Geosci. Model Dev.* **15**, 2973–3020 (2022).
633 71. Nijsse, F. J. M. M., Cox, P. M. & Williamson, M. S. Emergent constraints on transient
634 climate response (TCR) and equilibrium climate sensitivity (ECS) from historical warming in
635 CMIP5 and CMIP6 models. *Earth System Dynamics* vol. 11 737–750 (2020).
636 72. Dunne, J. P. *et al.* GFDL's ESM2 Global Coupled Climate–Carbon Earth System Models.
637 Part I: Physical Formulation and Baseline Simulation Characteristics. *J. Clim.* **25**, 6646–6665
638 (2012).
639 73. Arora, V. K. *et al.* Carbon–concentration and carbon–climate feedbacks in CMIP6 models
640 and their comparison to CMIP5 models. *Biogeosciences* **17**, 4173–4222 (2020).
641 74. Mauritsen, T. *et al.* Developments in the MPI-M Earth System Model version 1.2 (MPI-
642 ESM1.2) and Its Response to Increasing CO_2. *J. Adv. Model. Earth Syst.* **11**, 998–1038 (2019).
643 75. Reick, C. H. *et al.* JSBACH 3 - The land component of the MPI Earth System Model:
644 documentation of version 3.2. 4990986 (2021) doi:10.17617/2.3279802.

76. Sellar, A. A. *et al.* UKESM1: Description and Evaluation of the U.K. Earth System Model. *J. Adv. Model. Earth Syst.* **11**, 4513–4558 (2019).
77. McNeall, D., Robertson, E. & Wiltshire, A. Constraining the carbon cycle in JULES-ES-1.0. *Geosci. Model Dev.* **17**, 1059–1089 (2024).

Figure Legends

Figure 1. Schematic overview of this study's methodology. First, we detect local (i.e., grid-cell scale) forest decline with and without a structural transition from forest to another vegetation type. A structural transition occurs when the tree cover falls below a model-specific threshold that characterizes forest vegetation (=Forest threshold). Second, we classify the forest decline as either abrupt or gradual by fitting different types of regression models that capture abrupt or gradual change to the time series of tree cover fraction. Lastly, we identify the driver (land-use change or climate change) of local forest decline. This is achieved by applying a model-specific threshold to the local CO_2 flux from land-use change (=fLuc), which is a proxy for the degree of local land-use change. For visualization purposes, we show the whole time period from 1950 to 2100. However, in reality each methodological step is applied separately to the historical (1950-2014) and future (2015-2100) time series.

Figure 2. Basin-wide forest decline per driver for 1950-2100. Annual forest decline across the Amazon basin is shown for the two drivers, land-use change and climate change, and two pathways (SSP3-7.0 and SSP5-8.5). Forest decline is shown in relation to the deforested area fraction (relative to the 1950 forest area) from the LUH2 land-use forcing and the global warming level relative to 1850 (model average), respectively. The solid lines represent the model average and the shaded areas represent the model range.

Figure 3. Timing of non-linear intensification of the basin-wide forest decline due to climate change across four models for 2015-2100. The numbers represent the fraction of the 1950 forest area that is projected to decline for two pathways (SSP3-7.0 and SSP5-8.5). The thin lines depict the annual data, whereas the thick lines represent the (polynomial) trend. The vertical dashed lines mark the starting point of the non-linear forest decline.

Figure 4. Fraction of the basin-wide area of forest decline characterized by abrupt versus gradual decline for 1950-2100. The numbers indicate the 10-year average fraction of the regional area of forest decline (relative to 1950) caused by each driver (CC=climate change or LUC=land-use change) and characterized by either abrupt (=AB) or gradual (=GR) decline for two pathways (SSP3-7.0 and SSP5-8.5). The average across four models is shown in the first row and the individual models are shown in the second and third rows.

Figure 5. Intensity and timing of forest decline across the Amazon basin. (A) Forest decline (%) relative to the 1950 forest area. Red areas in the small insets emphasize locations where forest decline includes a structural transition from forest to other vegetation. (B) Intensity of forest decline relative to the 1950 forest area per driver. Intensity (low, med(ium), high) is classified for each driver (climate change=CC or land-use change=LUC) depending on the fractional area of forest decline between 1950 and 2100: low: >0-20%, medium: >20-40%, high: >40%. Stipplings represent areas where at least three out of four models agree on the driver of forest decline. (C) Timing of the largest forest decline. The timing is classified as the year with the largest forest decline between 1950 and 2100. All values in (A-C) represent the model average for two pathways (SSP3-7.0 and SSP5-8.5). The data for each model is regridded to a common horizontal resolution of 100km.

Tables

Table 1. Glossary of important terms used in this study.

Term	Definition
Forest decline	Reduction in tree cover fraction with or without structural transition
Forest decline with structural transition	Reduction in tree cover fraction that triggers a structural forest transition, i.e., a transition from forest to another vegetation type (e.g., savanna)
Forest decline without structural transition	Reduction in tree cover fraction that does not trigger a structural forest transition (i.e., forest stays forest)
Local forest decline	Forest decline at a specific grid cell (size of the grid cell depends on the spatial resolution of each ESM)
Basin-wide forest decline	Forest decline on the basin scale, calculated by summing the local forest decline across the Amazon basin
Resilience	The ability of an ecosystem (e.g., a forest) to recover from any type of disturbance[69]
Forest degradation	A transitory or long-term deterioration in forest conditions (e.g., properties, functions, services) without a change in land cover (forest stays forest). This can be caused by forest fires, logging and other drivers[8]
Deforestation	A conversion from forest to other land cover types, e.g. due to agricultural expansion[8]
Tipping point	A critical threshold at which a tiny perturbation can qualitatively alter the state or development of a system[23]

699 **Table 2.** Comparison of general features and relevant processes for forest disturbance and
700 mortality in the four Earth System Models used in this study. ESM=Earth System Model, Hor.
701 res.=horizontal resolution of the land surface scheme, Dyn. veg.=Dynamic vegetation, Nat. dist. =
702 Natural disturbance processes, TCR=Transient Climate Response, GWL=Global warming level.

ESM	**Hor. res. (km)**	**Number of ensemble members**	**Dyn. veg.**	**Nat. dist.**	**Land model**	**TCR (°C)**	**GWL at breakpoint of climate change impact (°C) (SSP3-7.0, SSP5- 8.5)**
EC-Earth3-Veg[70]	100	3	-Yes -Age-height cohorts included	-Natural fires -Wind throw - Pest attacks	LPJ-GUESS v4[36]	2.6[71]	3.9, 4.1
GFDL-ESM4[72]	100	1	-Yes -Age-height cohorts included	-Natural fires	LM4.1[37]	1.6[73]	3.0, 2.3
MPI-ESM1-2-LR[74]	250	29	-Yes -Age-height cohorts not included	-Natural fires -Wind throw	JSBACH 3.2[75]	1.9[73]	2.9, 3.1
UKESM1-0-LL[76]	250[73]	16	-Yes -Age-height cohorts not included		JULES-ES-1.0[77]	2.4[73]	4.6, 4.6

703

Table 3. Comparison of the area affected by structural transition from forest to other vegetation for 1985-2014 simulated by three Earth System Models and from observational data. The model-specific optimum tree cover threshold to define forest vegetation is chosen by comparing the historical forest area change from the LUH2 land-use forcing dataset to the ESM simulations. Note that GFDL-ESM4 is not included in the table since it was not possible to robustly quantify a tree cover threshold due to strong differences between the simulated historical forest area change and the LUH2 forcing dataset.

	Dataset	**Time period**	**Structural forest transition due to land-use change (km^2)**	**Fraction of structural forest transition due to land- use change (% of 1985 forest area)**	**Optimum tree cover threshold to define forest vegetation (%)**
Earth System Models	EC-Earth3-Veg[70]	1985-2014	140,930	3	40
	MPI-ESM1-2-LR[74]		437,000	7	75
	UKESM1-0-LL[76]		379,353	7	65
Observations	MapBiomas[34]		497,802	9	-

Detection of local forest decline

Forest decline without structural transition

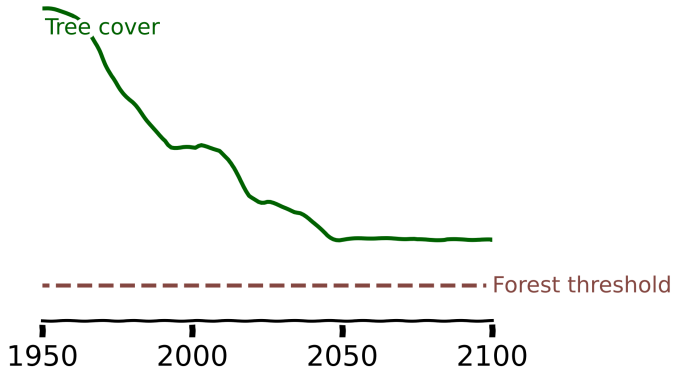

Forest decline with structural transition

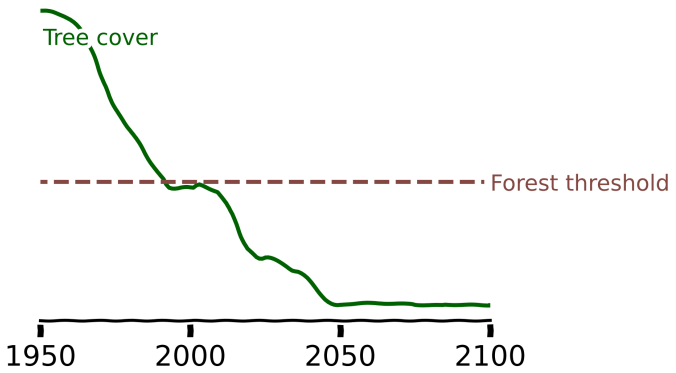

Classification of type of change

Gradual

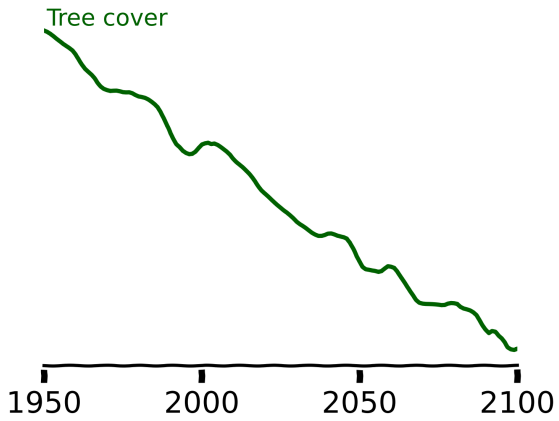

Abrupt

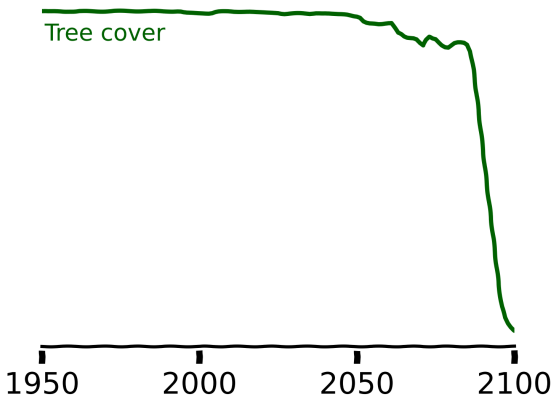

Attribution of driver of change

Land-use change

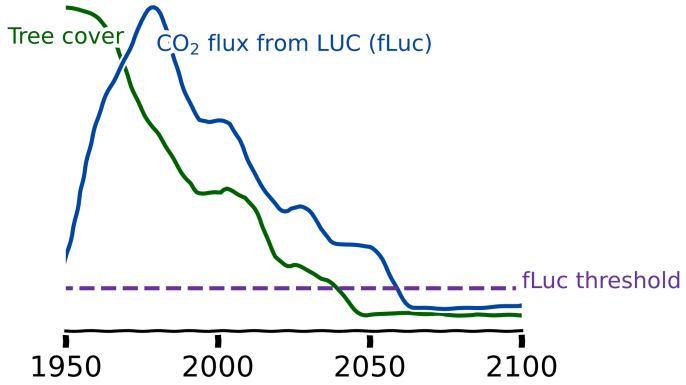

Climate change

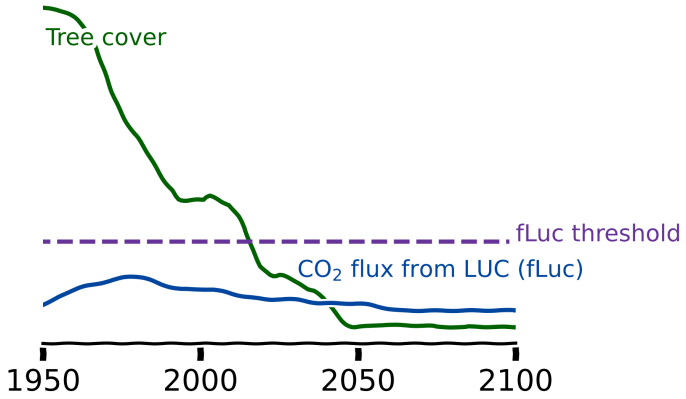

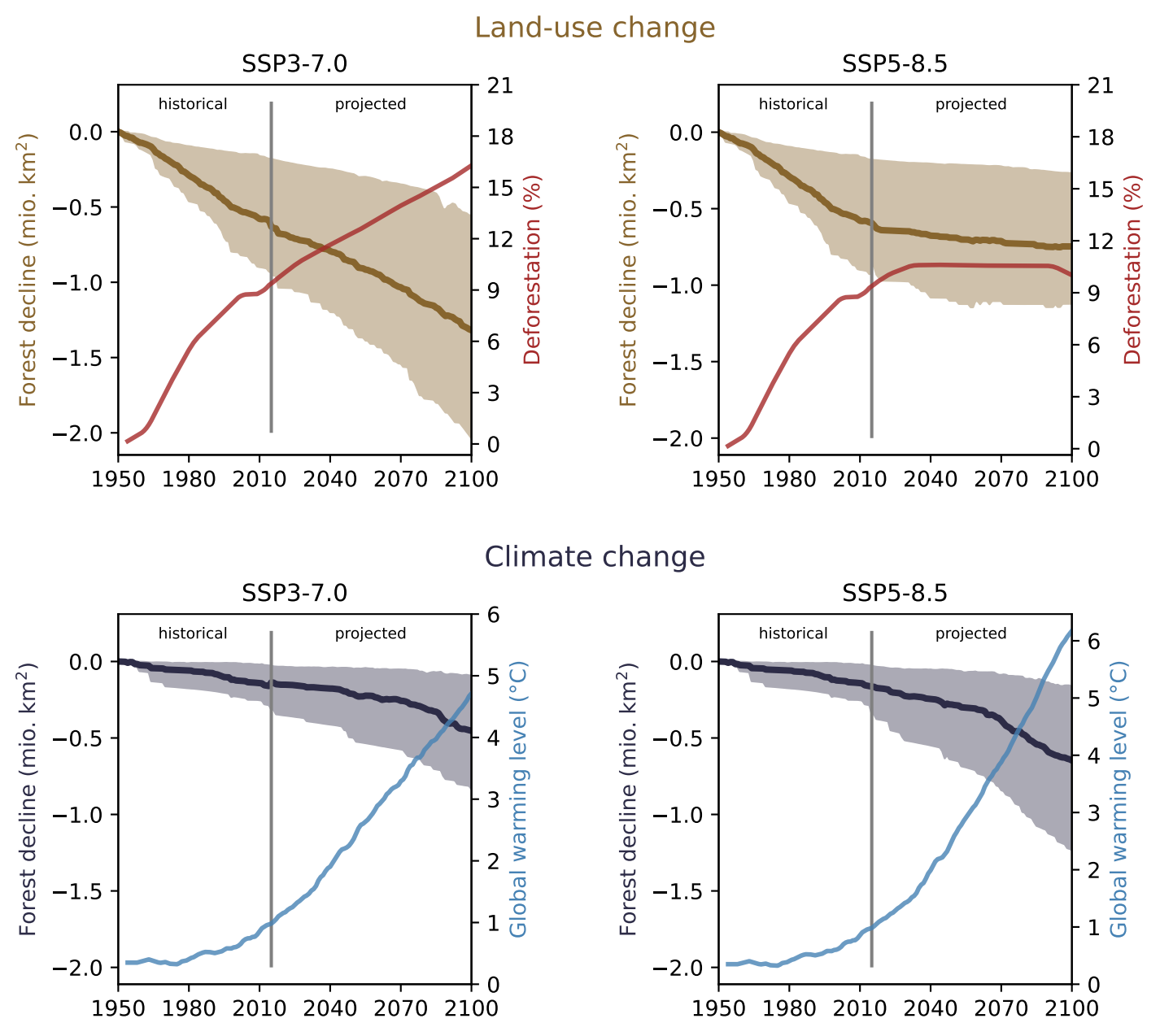
Land-use change
SSP3-7.0
SSP5-8.5
historical
projected
Forest decline (mio. km²)
Deforestation (%)
0.0
−0.5
−1.0
−1.5
−2.0
21
18
15
12
9
6
3
0
1950
1980
2010
2040
2070
2100
Climate change
SSP3-7.0
SSP5-8.5
historical
projected
Forest decline (mio. km²)
Global warming level (°C)
6
5
4
3
2
1
0

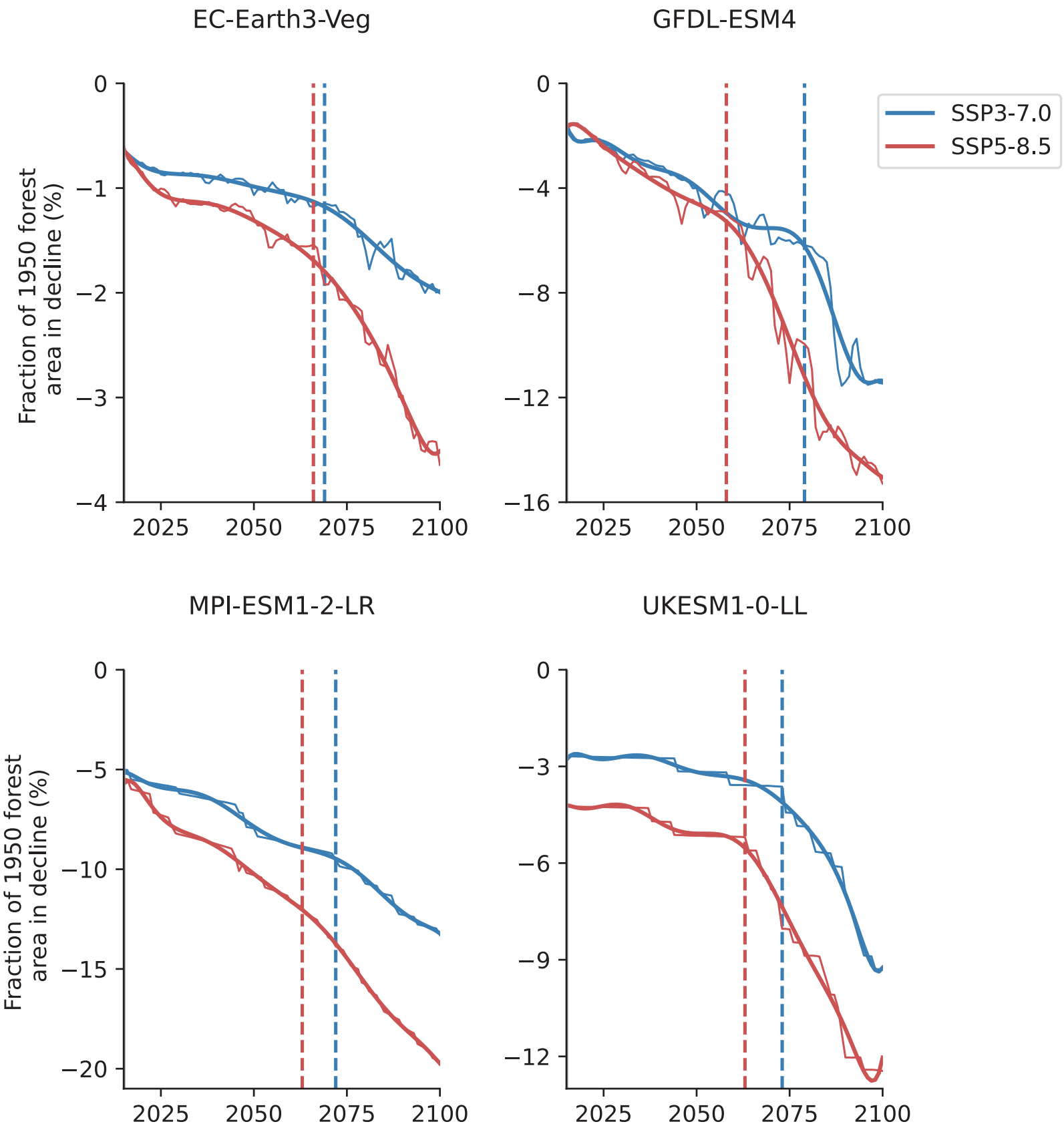
EC-Earth3-Veg
GFDL-ESM4
MPI-ESM1-2-LR
UKESM1-0-LL
Fraction of 1950 forest area in decline (%)
SSP3-7.0
SSP5-8.5
0
−1
−2
−3
−4
−8
−12
−16
−5
−10
−15
−20
−6
−9
2025
2050
2075
2100

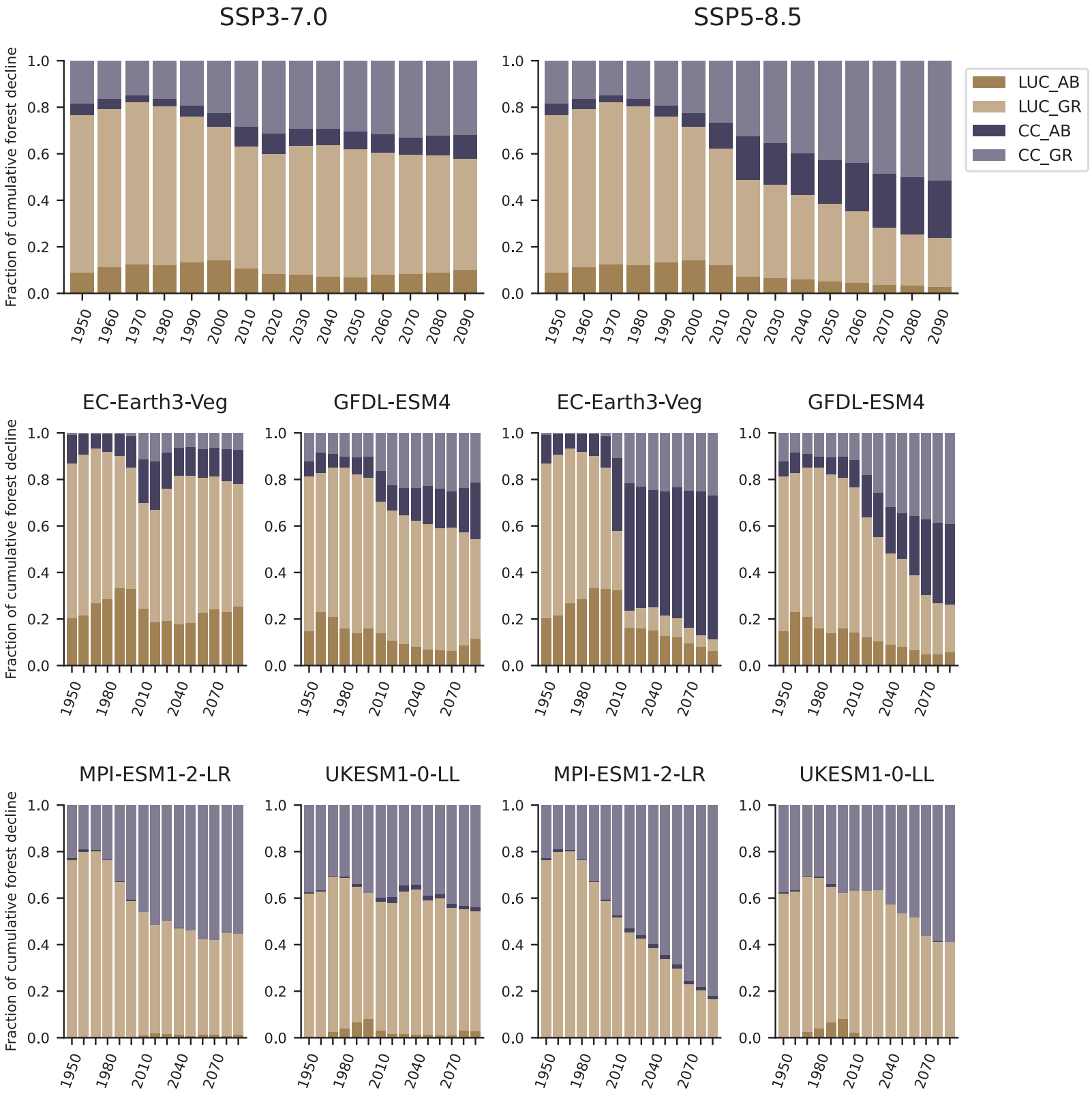
SSP3-7.0
SSP5-8.5
Fraction of cumulative forest decline
LUC_AB
LUC_GR
CC_AB
CC_GR
EC-Earth3-Veg
GFDL-ESM4
EC-Earth3-Veg
GFDL-ESM4
MPI-ESM1-2-LR
UKESM1-0-LL
MPI-ESM1-2-LR
UKESM1-0-LL

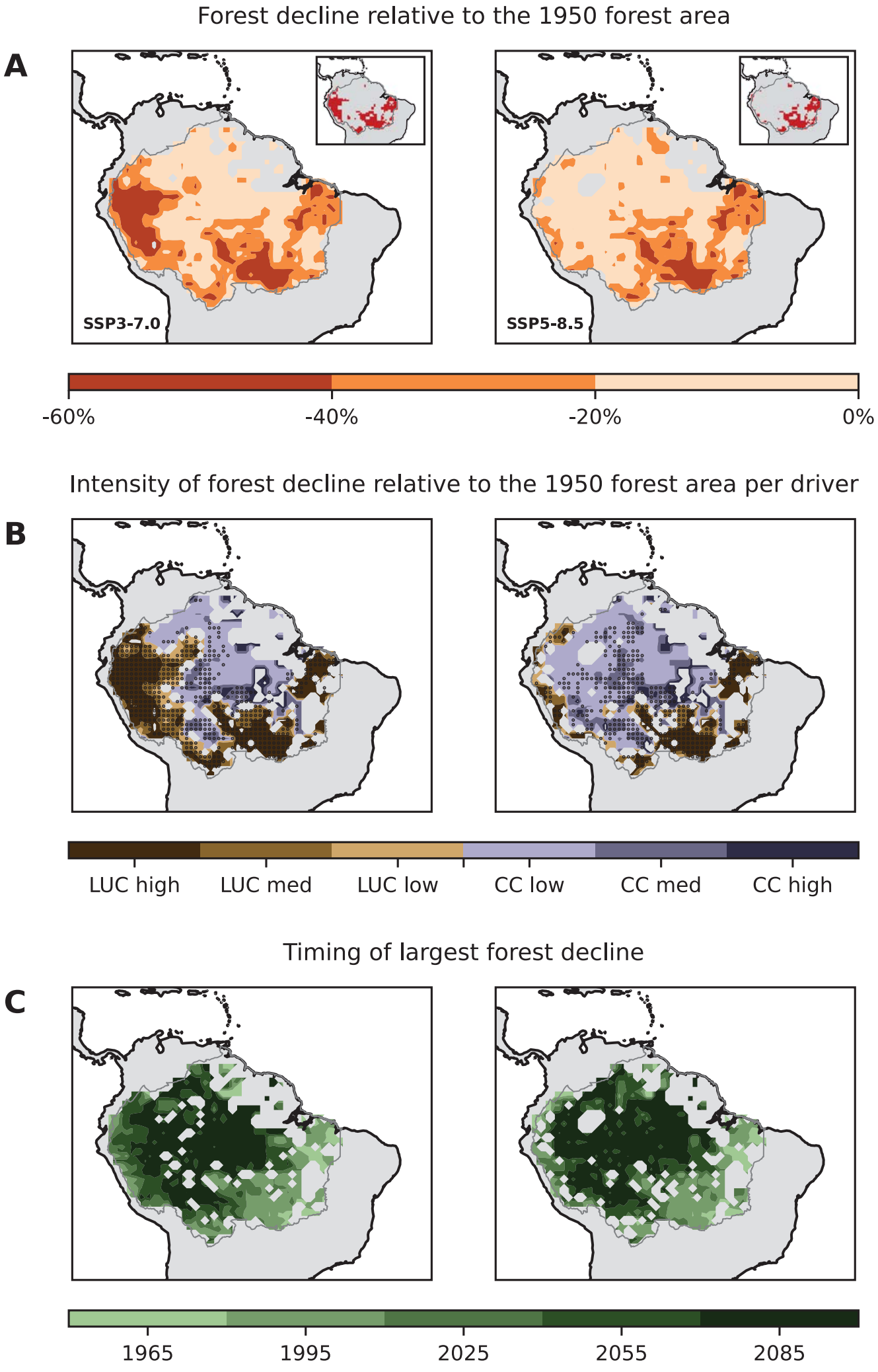
Forest decline relative to the 1950 forest area
A
SSP3-7.0
SSP5-8.5
-60%
-40%
-20%
0%
Intensity of forest decline relative to the 1950 forest area per driver
B
LUC high
LUC med
LUC low
CC low
CC med
CC high
Timing of largest forest decline
C
1965
1995
2025
2055
2085